

Dedicated

to

My Beloved

Maa-Deta

Dada-Bou

& Rig

DECLARATION BY THE CANDIDATE

I, Ms. Julie Baruah, Ph.D. Scholar (Regd no.:TZ189844 of 2018), Department of Chemical Sciences, Tezpur University, hereby, declare that the thesis entitled, “An Integrated Approach for Generation of Hydroxymethylfurfural Platform Chemical from Renewable Lignocellulosic Sources” has been submitted to the Department of Chemical Sciences, Tezpur University under the School of Sciences in partial fulfilment for the award of the degree of Doctor of Philosophy in Chemical Sciences. This is an original work carried out by me and it has not been previously considered for the award of any degree, diploma, associateship, fellowship or any other similar title or recognition from any University, Institute, or other organization.

I further declare that; I have duly acknowledged the support received from respective sources.

Date: 17/05/2023

Place: Tezpur, Assam



(Julie Baruah)

Regd no.:TZ189844 of 2018
Department of Chemical Sciences
School of Sciences, TU

Dr. Ramesh Ch. Deka, FRSC
Professor, Department of Chemical Sciences
Tezpur University,
Napaam -784028, Tezpur,
Assam, India.



NAAC Grade A+

Phone: 03712-275058 (O); 273639 (R) Fax: 03712-267005; Mobile: 9435380221; E-mail: ramesh@tezu.ernet.in


CERTIFICATE OF THE SUPERVISOR

This is to certify that the thesis entitled “*An Integrated Approach for Generation of Hydroxymethylfurfural Platform Chemical from Renewable Lignocellulosic Sources*” submitted by Ms. **Julie Baruah** to the School of Sciences, Tezpur University in partial fulfilment for the award of the degree of Doctor of Philosophy in **Chemical Sciences** is a record of bonafide research work carried out by her under my supervision and guidance. She has been duly registered, completed her Ph.D. course work and the thesis presented is worthy of consideration for the award of Ph.D. degree.

All help received by her from various sources have been duly acknowledged.

The contents of this thesis, in full or in part, have not been submitted to any other university for the award of any degree or diploma.

Date: 17/05/2023
Place: Tezpur, Assam


(Ramesh Ch. Deka)
Supervisor



কটন বিশ্ববিদ্যালয়
Cotton University

Department of Molecular Biology & Biotechnology
Panbazar, Guwahati, Assam-781001

Dr. Eeshan Kalita
Associate Professor

eeshan.kalita@cottonuniversity.ac.in, eeshankalita@gmail.com
+918638723313, +99435733617

CERTIFICATE OF THE CO-SUPERVISOR

This is to certify that the thesis entitled “*An Integrated Approach for Generation of Hydroxymethylfurfural Platform Chemical from Renewable Lignocellulosic Sources*” submitted to the School of Sciences, Tezpur University in partial fulfilment for the award of the degree of Doctor of Philosophy in **Chemical Sciences** is a record of original research work carried out by **Ms. Julie Baruah** under my personal supervision and guidance.

All help received by her from various sources have been duly acknowledged.

No part of this thesis has been submitted elsewhere for award of any other degree.

Date: 14-05-2023
Place: Guwahati, Assam

(Eeshan Kalita)
Co-supervisor



TEZPUR UNIVERSITY
(A Central University established by an Act of Parliament)
Napaam, Tezpur-784028, Sonitpur, Assam, India

Phone: +91-3712-267004 (O)

Fax: +91-3712-267005 (O)

CERTIFICATE OF THE EXTERNAL EXAMINER AND ODEC

This is to certify that the thesis entitled “*An Integrated Approach for Generation of Hydroxymethylfurfural Platform Chemical from Renewable Lignocellulosic Sources*” submitted by **Ms. Julie Baruah** to the School of Sciences, Tezpur University in partial fulfilment for the award of the degree of Doctor of Philosophy in **Chemical Sciences** has been examined by us on 17/05/2023 and found to be satisfactory.

The committee recommends for the award of the Degree of Doctor of Philosophy.

A handwritten signature in blue ink, appearing to read "Julie Baruah".

Principal supervisor

Date: 17/05/2023

A handwritten signature in blue ink, appearing to read "Dr. Paresh Dhepe".

Dr. Paresh Dhepe

External examiner

Date: 17/05/2023

ACKNOWLEDGEMENT

“One step at a time is all it takes to get you there.” This Ph.D. thesis is the outcome of my five wonderful years of research experience and ardent learning. The words on these pages are not merely words; they are what I genuinely feel for. I would like to acknowledge all the people, who, in their own ways, have helped me come this far.

At the very outset, I would like to express my sincere gratitude to my supervisor, Dr. Ramesh Chandra Deka, Professor, Department of Chemical Sciences, Tezpur University. I would remain ever debtful towards him for his immense faith in my capabilities, his intellectuality, and invaluable encouragement throughout my research journey. His calm and collected personality in every circumstance has inspired and taught me to deal with problems effectively. I consider myself fortunate to be a part of his research group.

I express my deep gratitude to my co-supervisor, Dr. Eeshan Kalita, Associate professor, Cotton University (Former Assistant professor of Department of MBBT, Tezpur University). I have completed all my experimental work in his laboratory. Words cannot express my thankfulness for his exceptional guidance, scientific supervision, and never-ending support, which served as the foundation of my whole research study. I am indeed grateful to be a part of his laboratory, whose devotion, hard work, and persistence have always motivated me to work hard and helped me sail past all the barriers. I shall remain indebted forever for all his contributions of time and commitment in making my research work a success.

I extend my sincere and hearty gratitude to my doctoral committee members, Prof. Debendra Chandra Baruah, Department of Energy, Tezpur University and Dr. Pankaj Bharali, Department of Chemical Sciences, Tezpur University for their constant inspiration and valuable suggestions during my research work.

I sincerely acknowledge the Heads, Department of Chemical Sciences (former Prof. Ruli Borah and present Prof. Panchanan Puzari) and Department of MBBT, (former Prof. Anand Ramteke and present Prof. Robin Doley) Tezpur University for providing the requisite facilities for conducting research work in both the department and for their kind assistance. I duly acknowledge all the faculty members of the Department of Chemical Sciences and Department of MBBT for their valuable advice and kind help. I am thankful

to all the technical and non-technical staff of both the departments for their assistance during the tenure.

I also thank the Dean, School of Sciences, Dean, Research and Development, and Controller of Examinations for all the support during my Ph.D. tenure.

I sincerely thank Prof. Manabendra Mandal, Department of MBBT, Tezpur University for giving me access of HPLC equipment in his laboratory and immensely grateful to his student Dr. Pritam Bardhan, currently research associate in the Department of MBBT, Tezpur University for his help in carrying out the HPLC analysis.

I would like to offer my sincere gratitude to Dr. Anil Kumar Sinha of IIP-Dehradun and his group for carrying out my Ammonia-TPD analysis.

I would like to offer my deepest gratitude to Dr. Nand Kishor Gour (Bhaiya) of Department of Chemical Sciences, Tezpur University, Dikshita Dowerah and Nishant Biswakarma for their valuable inputs and help in carrying out my computational work. I am always obliged to them in this aspect for training me the theoretical work.

I would also like to offer my earnest thanks to Dr. Ratan Boruah, Dr. Nipu Dutta, Mr. Sankur Phukan, Mr. Manoranjan Sarma, Mr. Biplab Ozah, Mr. Pranab Mudoji, Mr. Prakash Kurmi, Mr. Tridip R. Nath, and Mr. Biju Boro for their assistance during the instrumental analysis and Ms. Bobita Das and our office staff for their help in many aspects. I am grateful to all the staff of the administrative community of Tezpur University.

I am also thankful to Dr. Mehedi Hassan of IIT-Delhi for helping me with the SAXS analysis. I gratefully acknowledge CIF, IIT-Guwahati for carrying out the VSM analysis and SAIF, CSIR-NEIST for carrying out the BET analysis. Some of the BET analyses have also been carried out in our own department and I am always grateful in this regard to Sudakhina Saikia from whom I learned to operate the BET instrument.

I thank Department of Biotechnology (DBT), Government of India, for the Research Grant (Grant No. BT/PR16008/NER/95/47/2015) and Ministry of Education, Government of India, for the STARS project grant (Grant No. STARS/APR2019/NS/527/FS) for financial assistance to complete the research work.

I wholeheartedly thank my lab senior of Department of MBBT, Dr. Bikash Kar Nath and Dr. Chayanika Chaliha and my former labmates Plabita, Lukapriya, Tandrali, Jahangir, and Abhik for their kind support and assistance which contributed towards building a positive working environment. I owe my gratitude to Bikash da who have immensely helped me during my initial days of Ph.D. and have guided me throughout the journey. I consider myself fortunate enough to have Chayanika ba as my senior and friend

who has been my constant source of help, support and motivation, both professionally and personally, whenever I needed.

I would like to convey my special thanks to all the members of my CMM family of Department of Chemical Sciences. I am grateful to my seniors Dr. Nand Kishor Gour, Dr. Subrata Paul, Dr. Dharitri Das, Dr. Rasna Devi, Dr. Pangkita Deka, Dr. Plaban Jyoti Sharma, Dr. Satyajit Dey Baruah, Dr. Saheen Sehnaz Begum and my labmates Dikshita Dowerah, Sudakhina Saikia, Nishant Biswakarma, Partha Pratim Churi, Shilpa Neog, Shrutishree Sarma, Moumita Basumatary, Priyanka Dutta and Ambalika Phonglo who all made my research journey so lively. The time spent with them over the years is something I shall cherish for life.

They say friends do not thank each other. I must then thank my own good fortune to have people like Rakhee Saikia, Dr. Chiranjita Goswami, Priyankamoni Saikia, Lukapriya Dutta, Plabita Das, Sudhamoyee Katakya, Dr. Aditi Saikia, Dr. Prashurya Pritam Mudoi, Dr. Rituraj Das, Anurag Dutta, Raktim Abha Saikia, Rashmi Chetry, Kristi Kabyashree, and my Ph.D. batchmates for making my stay at Tezpur University a memorable and cheerful experience. A big thank you to Ravi Kumar Sahu for his constant help in many aspects throughout this journey.

I would like to express my special gratitude to Prof. Debendra Ch. Baruah and his family for the warm hospitality and affection bestowed upon me during my stay at Tezpur University.

No words can repay for the continuous encouragement, moral support, love, blessings, and everything else that I received from my parents, Binay Baruah and Dipali Baruah. No degree of thanks would ever justify the love, concern and support of my dearest brother, Pankaj Baruah and sister-in-law, Tinu Hazarika Baruah. I owe a lot to my little nephew, “Rig” (Alankrit Baruah) for adding joy and beauty in my life with his charms when I needed it most.

Last but not the least, I bow down to Almighty, who I believe to be with me every moment and showering his blessings upon me.

Julie Baruah

LIST OF FIGURES

<i>Figure No.</i>	<i>Figure legend</i>	<i>Page No.</i>
<u><i>Chapter 1</i></u>		
Fig. 1.1.	Number of publications on HMF annually from 1989 to 2021 (Source: Web of Science).	1.2
Fig. 1.2.	HMF as a platform chemical for the synthesis of various value-added chemicals.	1.3
Fig. 1.3.	Percentage composition of lignocellulosic sources.	1.4
Fig. 1.4.	Effect of pretreatment on lignocellulosic biomass.	1.5
<u><i>Chapter 2</i></u>		
Fig. 2.1.	Schematic structure of lignocellulose.	2.2
Fig. 2.2.	Flow chart diagram of pretreatment processes.	2.3
Fig. 2.3.	Interruption of intra- and intermolecular H-bonding in cellulose by ILs.	2.10
Fig. 2.4.	Two pathways postulated for the glucose-to-HMF conversion.	2.19
Fig. 2.5.	Routes to major side products after producing HMF from sugar dehydration.	2.21
Fig. 2.6.	Biphasic solvent system for the dehydration of carbohydrates to HMF.	2.25
<u><i>Chapter 3</i></u>		
Fig. 3.1.	<i>S. spontaneum</i> (Kans grass) (a), Banana (<i>Musa</i> spp.) Dwarf Cavendish (local name: “Jahaji”) stem (b) peel (c) peduncle (d) their respective chopped and dried samples (a’, b’, c’, and d’), and respective milled samples (a’’, b’’, c’’, and d’’).	3.4
Fig. 3.2.	Schematic representation of the procedure for the extraction of cellulose.	3.5
Fig. 3.3.	Comparison of the native lignocellulosic content in various feedstocks w.r.t. <i>S. spontaneum</i> and banana agrowastes (this work) (a); cellulose recovery and lignocellulosic residues after cellulose isolation using the ammonia/chlorine-free, mild acid-treated integrated approach (<i>S. spontaneum</i> , banana peduncle, pseudostem, peel) (this work), 5% H ₂ SO ₄ treatment at 170 °C (pine residual sawdust), alkaline-acid treatment followed by	3.11

chlorination and bleaching (coconut fiber and rice straw), microwave-assisted alkaline delignification (banana peduncle) and acetylation treatment containing 60% H₂SO₄ (banana peduncle) (b); comparative table representing the percentage composition of lignocellulosic components before and after cellulose extraction (c).

- Fig. 3.4.** FTIR spectra of *S. spontaneum* (a), banana pseudostem (b), banana peel (c), and banana peduncle (d) at different stages of treatment. 3.13
- Fig. 3.5.** XRD spectra of *S. spontaneum* (a), banana pseudostem (b), banana peel (c), and banana peduncle (d) at different stages of treatment. 3.15
- Fig. 3.6.** TGA curves (a, d, g, j), DTG curves (b, e, h, k), and thermal analysis data (c, f, i, l) of *S. spontaneum*, banana pseudostem, banana peel, and banana peduncle at various phases of treatment. [#]TGA initial decomposition temperature, ^{*}DTG peak temperature, [©]TGA maximum weight loss, ^uTGA char residue weight. 3.17
- Fig. 3.7.** SEM images of *S. spontaneum* (a), banana pseudostem (b), banana peel (c), and banana peduncle (d) at different stages of pretreatment. 3.19
- Fig. 3.8.** XRD spectra of nine cellulose samples obtained under different hydrolysis conditions from *S. spontaneum* (a) and banana peduncle (b). 3.23
- Fig. 3.9.** TGA and DTG curves of nine cellulose samples obtained from *S. spontaneum* (a and c) and from banana peduncle (b and d) under different hydrolysis conditions. 3.26

Chapter 4

- Fig. 4.1.** Schematic representation of the complete enzymatic hydrolysis procedure. 4.4
- Fig. 4.2.** Architectures for the glucose yield prediction model by ANN (a) and ANFIS (b). 4.7
- Fig. 4.3.** Effect of univariate interactions described by the model on the glucose yield for *S. spontaneum* cellulose. 4.13
- Fig. 4.4.** Effect of multivariate interactions: Response surface 3D plots (a-c) and response surface contour plots (a'-c') described by the model on the glucose yield for *S. spontaneum* cellulose. 4.13
- Fig. 4.5.** Effect of univariate interactions described by the model on the glucose yield for banana peduncle cellulose. 4.17

Fig. 4.6.	Effect of multivariate interactions: Response surface 3D plots (a-d) and response surface contour plots (a'-d') described by the model on the glucose yield for banana peduncle cellulose.	4.17
Fig. 4.7.	Pareto graphic analysis and normal probability plot described by the models for <i>S. spontaneum</i> cellulose (a, c) and for banana peduncle (b, d), respectively.	4.18
Fig. 4.8.	Selection of the best ANN architecture based on the determination coefficients (R^2) for <i>S. spontaneum</i> cellulose (a), banana peduncle cellulose (c) and mean squared error (MSE) values for <i>S. spontaneum</i> cellulose (b), banana peduncle cellulose (d) for the training and validation of the optimum ANN topology.	4.20
Fig. 4.9.	Membership function plots of input variables for <i>S. spontaneum</i> cellulose model (a) and banana peduncle cellulose model (b).	4.21
Fig. 4.10.	3D surface plots described by the ANFIS models for <i>S. spontaneum</i> cellulose (a-c) and for banana peduncle cellulose (d-g) on the glucose yield.	4.23
Fig. 4.11.	ANFIS rule viewer for the effect of process variables on responses for enzymatic hydrolysis of <i>S. spontaneum</i> (a) and banana peduncle (b).	4.24
Fig. 4.12.	Comparison of predictive outputs of RSM, ANN and ANFIS design matrices based on determination coefficients for <i>S. spontaneum</i> model (a) and banana peduncle model (b).	4.25
Fig. 4.13.	Glucose standard curve of HPLC (a); HPLC chromatograms showing the glucose peaks at optimal conditions of RSM, ANN and ANFIS obtained from <i>S. spontaneum</i> cellulose (b) and banana peduncle cellulose (c).	4.27

Chapter 5

Fig. 5.1.	Schematic representation of x-Fe ₃ O ₄ @SPAN-y/z synthesis.	5.4
Fig. 5.2.	Comparative analysis of the catalytic activity of different catalysts (a), effect of Fe ₃ O ₄ wt% loading on the glucose conversion and HMF yield (b), effect of sulfate functionalization on 15-Fe ₃ O ₄ @SPAN-y/z catalyst (c), effect of different single-phase and biphasic solvents on the glucose conversion and HMF yield (d), influence of the inorganic phase to organic phase (MIBK) ratio on the glucose conversion and HMF yield (e) (reaction conditions: 80 mM glucose, 40 mg 15-Fe ₃ O ₄ @SPAN-9/3, 150 °C, 4h).	5.10
Fig. 5.3.	FTIR spectra of the synthesized catalysts (a) and magnified view of the absorption band area of PANI, SPAN and 15-Fe ₃ O ₄ @SPAN-9/3 from 2000-400 cm ⁻¹ (b).	5.12

Fig. 5.4.	XRD patterns (a) and Raman spectra (b) of the synthesized catalysts.	5.13
Fig. 5.5.	TGA and DTG curves of PANI (a), Fe ₃ O ₄ np (b), and 15-Fe ₃ O ₄ @SPAN-9/3 catalyst (c).	5.14
Fig. 5.6.	NH ₃ -TPD analysis of the synthesized catalysts (a), and VSM magnetization curves of Fe ₃ O ₄ nanoparticles and 15-Fe ₃ O ₄ @SPAN-9/3 catalyst (b).	5.15
Fig. 5.7.	XPS survey scan of 15-Fe ₃ O ₄ @SPAN-9/3 (a); high resolution XPS spectra of Fe(2p) (b), C(1s) (c), N(1s) (d), O(1s) (e), and S(2p) (f).	5.17
Fig. 5.8.	SEM micrographs of PANI (a), Fe ₃ O ₄ (b), and 15-Fe ₃ O ₄ @SPAN-9/3 (c); EDX spectrum of 15-Fe ₃ O ₄ @SPAN-9/3 (d); elemental distribution table (d inset); and pseudo-colour elemental distribution maps of 15-Fe ₃ O ₄ @SPAN-9/3 (e-i).	5.18
Fig. 5.9.	Low magnification TEM images (a, b), HRTEM image (c, d), the SAED pattern (e), and the corresponding particle size distribution for 15-Fe ₃ O ₄ @SPAN-9/3 (f). The white and yellow arrows in (b) show the existence of PANI and Fe ₃ O ₄ nanoparticles.	5.19
Fig. 5.10.	Nitrogen adsorption-desorption isotherms and the corresponding pore size distribution curves (insets) of PANI (a), SPAN (b), Fe ₃ O ₄ (c) and 15-Fe ₃ O ₄ @SPAN-9/3 (d).	5.20
Fig. 5.11.	Effect of univariate interactions defined by the CCD-RSM model on the HMF yield (a-d); effect of multivariate interactions: response surface 3D plots (e-g) and the corresponding contour plots (e'-g') defined by the CCD-RSM model on the HMF yield.	5.25
Fig. 5.12.	Normal probability plot (a), predicted vs. actual plot (b) and Pareto graphic analysis described by the model.	5.26
Fig. 5.13.	Selection of the best ANN architecture based on mean squared error (MSE) values (a) and the determination coefficients (R ²) (b); comparison of the predictive outputs of RSM and ANN models based on determination coefficients (c) and distribution of residuals (d).	5.28
Fig. 5.14.	HMF standard curve of HPLC (a); HPLC chromatograms showing the HMF peaks at optimal conditions of RSM and ANN (b); magnified view of the HPLC chromatogram (b inset); HPLC chromatograms showing the HMF peaks from <i>Saccharum spontaneum</i> derived glucose (c), and banana peduncle derived glucose (d); magnified view of the HPLC chromatograms (c inset, d inset). (Reaction condition: 80 mMol glucose, 40 mg catalyst, 150 °C, 4h).	5.31

Fig. 5.15	Catalyst recycling of 15-Fe ₃ O ₄ @SPAN-9/3 (Reaction conditions: 40 mg catalyst, 80 mMol glucose, 150 °C, and 4h) (a), comparison of FTIR spectrum of 15-Fe ₃ O ₄ @SPAN-9/3 and fifth used 15-Fe ₃ O ₄ @SPAN-9/3 catalyst (b), SEM-EDX spectrum of fifth used 15 Fe ₃ O ₄ @SPAN-9/3 catalyst (c), and TGA/DTG plots of the fresh and fifth used catalyst (d).	5.33
Fig. 5.16.	Mechanism proposed for the catalytic dehydration of glucose to HMF using x-Fe ₃ O ₄ @SPAN-y/z-based catalyst.	5.35
Fig. 5.17.	Optimized structure of all the species (of proposed mechanism) obtained at B3LYP/LANL2DZ level of theory.	5.38
Fig. 5.18.	Potential energy diagram for the dehydration of glucose to HMF using Fe ₃ O ₄ @SPAN obtained at at B3LYP/LANL2DZ level of theory.	5.41

Chapter 6

Fig. 6.1.	Schematic representation of the synthetic procedure of Nb-KIT-6-SO ₃ H catalyst.	6.4
Fig. 6.2.	Comparative analysis of the catalytic activity of Nb-KIT-6-SO ₃ H with pure silica KIT-6 and non-functionalized Nb-KIT-6 (a), the effect of molar ratio of Si/Nb loading on the catalytic activity of Nb-KIT-6(x)-SO ₃ H catalysts (b), effect of different single-phase and biphasic solvents on the glucose conversion and HMF yield (c), the influence of the inorganic phase to organic phase (MIBK) ratio on the glucose conversion and HMF yield (d), and influence of NaCl concentrations on the glucose conversion and HMF yield (e). (Reaction conditions: 40 mM glucose, 40 mg catalyst, 120 °C, 60 min).	6.11
Fig. 6.3.	FTIR spectra (a) and p-XRD patterns (b) of KIT-6, Nb-KIT-6 with Si/Nb ratio 20 and Nb-KIT-6(x)-SO ₃ H samples, where x is the Si/Nb ratio.	6.13
Fig. 6.4.	Small angle X-ray scattering patterns (a) and Diffuse reflectance UV–vis spectra (b) of Nb-KIT-6(x)-SO ₃ H samples.	6.14
Fig. 6.5.	TGA curves of pure KIT-6, Nb-KIT-6, and Nb-KIT-6(20)-SO ₃ H.	6.15
Fig. 6.6.	Nitrogen adsorption-desorption isotherms (a) and the corresponding pore size distribution curves (b) of KIT-6, Nb-KIT-6 with Si/Nb ratio 20, and Nb-KIT-6(x)-SO ₃ H samples, where x is the Si/Nb ratio.	6.16
Fig. 6.7.	NH ₃ -TPD analysis of KIT-6, Nb-KIT-6, and Nb-KIT-6(20)-SO ₃ H (a) and fitting curve of Nb-KIT-6(20)-SO ₃ H (b).	6.17

Fig. 6.8.	XPS survey scan of Nb-KIT-6(20)-SO ₃ H (a); high resolution XPS spectra of Si (2p) (b), Nb (3d) (c), O (1s) (d), S (2p) (e), and C (1s) (f).	6.19
Fig. 6.9.	SEM micrographs of KIT-6 (a), Nb-KIT-6 (b), and Nb-KIT-6(20)-SO ₃ H (c); EDX spectrum of KIT-6 (d), Nb-KIT-6 (e), and Nb-KIT-6(20)-SO ₃ H (f); elemental distribution table (d, e and f insets); and pseudo-colour elemental distribution maps of KIT-6 (g, h), Nb-KIT-6 (i-k), and Nb-KIT-6(20)-SO ₃ H (l-o).	6.20
Fig. 6.10.	HRTEM images of KIT-6 (a, d, and g), Nb-KIT-6 (b, e, and h), and Nb-KIT-6(20)-SO ₃ H (c, f, and i) at 10 nm, 20nm, and 50 nm resolution; the corresponding pore size distribution curves of KIT-6 (a inset), Nb-KIT-6 (d inset) and Nb-KIT-6(20)-SO ₃ H (g inset).	6.21
Fig. 6.11.	Effect of univariate interactions defined by the CCD-RSM model on the HMF yield (a-d).	6.25
Fig. 6.12.	Effect of multivariate interactions: response surface 3D plots (a-d) and the corresponding contour plots (a'-d') defined by the CCD-RSM model on the HMF yield.	6.26
Fig. 6.13.	Normal probability plot (a), predicted vs. actual plot (b), and Pareto graphic analysis described by the model.	6.27
Fig. 6.14.	Selection of the best ANN architecture based on mean squared error (MSE) values (a) and the determination coefficients (R ²) (b); comparison of the predictive outputs of RSM and ANN models based on determination coefficients (c) and distribution of residuals (d).	6.29
Fig. 6.15.	Glucose standard curve of HPLC (a); HMF standard curve of HPLC (b); HPLC chromatograms showing the HMF peaks in aqueous phase (c, d) and in organic (MIBK) phase (e, f) from <i>Saccharum spontaneum</i> derived glucose and banana peduncle derived glucose, respectively. (Reaction condition: 60 mMol glucose, 30 mg catalyst, 150 °C, 60 min).	6.32
Fig. 6.16.	Catalyst recycling of Nb-KIT-6(20)-SO ₃ H (Reaction conditions: 30 mg catalyst, 60 mMol glucose, 150 °C, and 60 min) (a), comparison of FTIR spectrum of fresh and fifth used Nb-KIT-6(20)-SO ₃ H catalyst (b), SEM-EDX spectrum of fifth used Nb-KIT-6(20)-SO ₃ H catalyst (c), and TGA plots of the fresh and fifth used Nb-KIT-6(20)-SO ₃ H catalyst (d).	6.33
Fig. 6.17.	Mechanism proposed for the catalytic dehydration of glucose to HMF using Nb-KIT-6(20)-SO ₃ H catalyst.	6.35

LIST OF TABLES

<i>Table No.</i>	<i>Table legend</i>	<i>Page No.</i>
<u><i>Chapter 3</i></u>		
Table 3.1.	Factors and their corresponding levels for the design of experimentations.	3.6
Table 3.2.	L9 orthogonal array scheme of Taguchi design.	3.6
Table 3.3.	Chemical composition of the primary constituents of <i>S. spontaneum</i> , banana pseudostem, banana peel, and banana peduncle at different stages of treatment.	3.11
Table 3.4.	Crystallinity index (CrI) value of <i>S. spontaneum</i> (a), banana pseudostem (b), banana peel (c), and banana peduncle (d) at different stages of treatment.	3.16
Table 3.5.	A comparison of the different alkaline, bleaching and hydrolysis conditions for obtaining cellulose with diverse yields, crystallinity index and thermal stabilities from reported studies.	3.18
Table 3.6.	Yield, molecular weight (Mw) and degree of polymerization (DP) of nine (09) cellulose samples obtained from <i>S. spontaneum</i> under different hydrolysis conditions.	3.21
Table 3.7.	Yield, molecular weight (Mw) and degree of polymerization (DP) of nine (09) cellulose samples obtained from banana peduncle under different hydrolysis conditions.	3.21
Table 3.8.	Crystallinity parameters of nine cellulose samples of <i>S. spontaneum</i> obtained under different hydrolysis conditions.	3.24
Table 3.9.	Crystallinity parameters of nine cellulose samples of banana peduncle obtained under different hydrolysis conditions.	3.24
Table 3.10.	Weight loss and degradation temperatures of nine cellulose samples obtained from <i>S. spontaneum</i> and banana peduncle under different hydrolysis conditions.	3.27
<u><i>Chapter 4</i></u>		
Table 4.1.	<i>Coded levels of variables for CCD.</i>	4.5
Table 4.2.	<i>Statistical error functions.</i>	4.8
Table 4.3.	Central composite design matrix, ANN, and ANFIS for the four independent variables on the glucose yield from <i>S. spontaneum</i> cellulose with predicted and actual response.	4.11

Table 4.4.	ANOVA for the fitted quadratic polynomial model for glucose yield of <i>S. spontaneum</i> cellulose.	4.12
Table 4.5.	Central composite design matrix, ANN and, ANFIS for the four independent variables on the glucose yield from banana peduncle with the predicted and actual responses.	4.15
Table 4.6.	ANOVA for the fitted quadratic polynomial model for glucose yield of banana peduncle cellulose.	4.16
Table 4.7.	Statistical error indices of RSM, ANN, and ANFIS.	4.26
Table 4.8.	Table of validation of optimal conditions predicted by RSM, ANN and ANFIS.	4.27
Table 4.9.	An assessment of diverse pretreatment and enzymatic hydrolysis procedures to obtain glucose with different yields from reported studies.	4.28

Chapter 5

Table 5.1.	Total acidity of PANI, Fe ₃ O ₄ nanoparticles and 15- Fe ₃ O ₄ -SPAN-9/3 catalyst.	5.15
Table 5.2.	Magnetic parameters of Fe ₃ O ₄ nanoparticles and 15-Fe ₃ O ₄ -SPAN-9/3 catalyst.	5.16
Table 5.3.	BET analysis data of the different catalysts.	5.20
Table 5.4.	Coded levels of variables for CCD Response Surface Methodology.	5.21
Table 5.5.	CCD and ANN matrix for the four independent variables on the HMF yield with predicted and actual response.	5.22
Table 5.6.	ANOVA for the fitted quadratic polynomial model for HMF yield.	5.24
Table 5.7.	Statistical error functions.	5.27
Table 5.8.	Statistical error indices of RSM and ANN.	5.29
Table 5.9.	Catalytic conversion of various glucose to HMF with 15-Fe ₃ O ₄ @SPAN-9/3 catalyst. Reaction condition: 80 mMol glucose, 40 mg catalyst, 150 °C, 4h.	5.31
Table 5.10.	Catalytic activity comparison of 15-Fe ₃ O ₄ @SPAN-9/3 with other reported catalysts.	5.36
Table 5.11.	Absolute value of total energy, enthalpy and Gibbs free energy of all the species calculated at the B3LYP/LANL2DZ level of theory. (Values are given in Hartree)	5.39
Table 5.12.	Standard reaction enthalpy (Δ_rH^0) and Gibbs free energy (Δ_rG^0) for the reaction steps at B3LYP/LANL2DZ level of theory. (Values are given in kcal/mol)	5.39

Table 5.13.	Relative energy of all the species with respect to SPAN, Fe ₃ O ₄ and Glucose calculated at the B3LYP/LANL2DZ level of theory.	5.40
--------------------	--	------

Chapter 6

Table 6.1.	BET analysis data of KIT-6, Nb-KIT-6 with Si/Nb ratio 20 and Nb-KIT-6(x)-SO ₃ H samples, where x is the Si/Nb ratio.	6.16
Table 6.2.	Total acidity of KIT-6, Nb-KIT-6, and Nb-KIT-6(20)-SO ₃ H.	6.18
Table 6.3.	Coded levels of variables for CCD Response Surface Methodology.	6.22
Table 6.4.	CCD and ANN matrix for the four independent variables on the HMF yield with the predicted and actual response.	6.23
Table 6.5.	ANOVA for the fitted quadratic polynomial model for HMF yield.	6.24
Table 6.6.	Statistical error functions.	6.27
Table 6.7.	Statistical error indices of RSM and ANN.	6.30
Table 6.8.	Catalytic conversion of various glucose to HMF with Nb-KIT-6(20)-SO ₃ H catalyst. Reaction condition: 60 mMol glucose, 30 mg catalyst, 150 °C, 60 min.	6.31
Table 6.9.	Comparison of catalytic performance of Nb-KIT-6(20)-SO ₃ H with other reported silica-based catalysts.	6.36

LIST OF ABBREVIATIONS AND SYMBOLS

[AMIM]Cl	1-Allyl-3-methylimidazolium chloride
[EMIM]BF ₄	1-ethyl-3-methylimidazolium tetrafluoroborate
[EMIM]Br	1-ethyl-3-methylimidazolium bromide
[EMIM]Cl	1-ethyl-3-methylimidazolium chloride
3-DG	3-Deoxyglucosone
AARE	Absolute average relative error
Adj R ²	Adjusted R ²
AFEX	Ammonia fiber explosion
AlPO	Aluminium phosphate
AN	Aniline
ANFIS	Adaptive neuro-fuzzy inference system
ANN	Artificial neural network
ANOVA	Analysis of variance
APS	Ammonium persulfate
ARE	Average relative error
B3LYP	Becke, 3-parameter, Lee–Yang–Parr
BET	Brunauer-Emmett-Teller
BJH	Barrett-Joyner-Halenda
BTU	British thermal units
BuOH	n-Butanol
C ₂ H ₂ O ₄	Oxalic acid
C ₂ H ₄ O ₂	Acetic acid
C ₆ H ₈ O ₇	Citric acid
CCD	Central composite design
CePO	Cerium phosphate
ChCl	Cholin chloride
ChOAc	Choline acetate
CrI	Crystallinity index
CSA	Carbon-based solid acid
DES	Deep eutectic solvents
DFT	Density functional theory

DMA	Dimethylacetamide
DMF	Dimethylformamide
DMSO	Dimethyl sulfoxide
DP	Degree of polymerization
DTG	Derivative thermogram
EDX	Energy Dispersive X-ray Diffraction spectroscopy
emu	Unit for magnetic moment
eV	Electronvolt
FDCA	2,5-Furandicarboxylic acid
Fe ₃ O ₄	Magnetite/ Iron (II, III) oxide
FeCl ₃ .6H ₂ O	Ferric chloride
FeCl ₄ .H ₂ O	Ferrous chloride tetrahydrate
FePO	Iron phosphate
FPU	Filter paper unit
FTIR	Fourier transform infrared
g	Gram
GVL	γ-Valerolactone
h	Hour
H ₂ N(CH ₂) ₆ NH ₂	1,6-hexanediamine
H ₂ O ₂	Hydrogen peroxide
H ₂ SO ₄	Sulphuric acid
H ₃ PO ₄	Orthophosphoric acid
HBD	Hydrogen bond donor
Hc	Negligible coercivity
HCl	Hydrochloric acid
HCW	Hot compressed water
HfPO	Hafnium phosphate
HMF	5-hydroxymethylfurfural
HNO ₃	Nitric acid
HPA	Heteropoly acids
HPLC	High-performance liquid chromatography
HRTEM	High resolution transmission electron microscopy
HYBRID	Hybrid fractional error function

ICP-AES	Inductively coupled plasma atomic emission spectroscopy
ILs	Ionic liquids
IUPAC	International Union of Pure and Applied Chemistry
KBr	Potassium Bromide
LA	Levulinic acid
LCB	Lignocellulosic biomass
LHW	Liquid Hot Water
LiP	Lignin peroxidase
LM	Levenberg Marquardt
M	Molar
MA	Metanillic acid
MCSC	Macroporous carbonaceous solid catalysts
MF	Membership functions
mg	Milligram
MIBK	Methyl isobutyl ketone
min	Minute
mL	Millilitre
MLP	Multi-Layered- Perceptron
mMol	Millimole
MMT	Montmorillonite
MMT	Million metric tonnes
MnP	Manganese peroxidase
MnPO	Manganese phosphate
MPSED	Marquardt's percent standard error deviation
MPTMS	3-mercaptopropyltrimethoxysilane
M_r	Remanent magnetization
M_s	Saturation magnetization
$\text{Na}_3\text{C}_6\text{H}_5\text{O}_7$	Sodium citrate
NaOH	Sodium hydroxide
NbCl_5	Niobium pentachloride
NbO_2	Niobium dioxide
NbPO	Niobium phosphate
NH_3 -TPD	Ammonia - Temperature programmed desorption

nm	Nanometre
NMMO	N-methylmorpholine-N-oxide
NMP	N-methyl pyrrolidone
OPMF	Oil palm mesocarp fiber
PANI	Polyaniline
R ²	Correlation coefficient
RMSE	Root mean squares error
rpm	Revolutions per minute
RSM	Response surface methodology
SAED	Selected area electron diffraction
SAXS	Small-angle X-ray scattering
SEM	Scanning electron microscope
SnPO	Tin phosphate
-SO ₃ H	Sulfonic acid groups
SPAN	Sulfonated polyaniline
SSB	Sweet sorghum bagasse
TAPPI	Technical Association of Pulp and Paper Industry
TEOS	Tetraethyl orthosilicate
TGA	Thermogravimetric Analysis
THF	Tetrahydrofuran
TiO ₂	Titanium dioxide
TiPO	Titanium phosphate
UV-vis	Ultraviolet-Visible spectroscopy
VP	Versatile peroxidase
VP	Versatile peroxide
VPO	Vanadium phosphate
VSM	Vibrating Sample Magnetometer
XPS	X-ray photoelectron spectroscopy
XRD	X-ray Diffraction
ZrO ₂	Zirconium dioxide
ZrPO	Zirconium phosphate
$\Delta_r G^\circ$	Gibbs free energy
$\Delta_r H^\circ$	Enthalpy